Testing Specific Theories Beyond General Relativity with LIGO

Natalie Malagon, Mentor: Ethan Payne

September 21, 2023

Abstract

Gravitational waves observed by LIGO allow us to test general relativity in the strong-field regime with populations of binary merger events. Observations thus far are consistent with general relativity at both the individual and population level. Current tests of general relativity utilize a single deviation parameter rather than generic deviation parameters, which makes it difficult to map this information to specific theories and robustly test them over ensembles of events. We apply Bayesian inference to the inspiral phase of gravitational-wave signals in binary black hole merger events, to obtain posterior distributions for the 15 source parameters and 10 post-Newtonian deviation parameters. This parameter estimation involves the hybrid sampling method which uses nested sampling to seed parallel-tempered Markov Chain Monte Carlo (MCMC) ensembles and allows us to explore degenerate parameter spaces. We apply a Principal Component Analysis (PCA) to reduce the dimensionality of the parameter space, to understand the underlying correlations between the deviation parameters. Hierarchical inference could then be applied to ensembles of events to test specific theories beyond general relativity, such as the dynamical Chern Simons (dCS) and Einstein-dilaton Gauss-Bonnet (EdGB) theories. This would result in constraining the bounds on the coupling coefficients that characterize these specific theories.

I. Introduction

The Laser Interferometer Gravitational-Wave Observatory (LIGO) has opened up a new era of physics with its first observation of a binary black hole merger [1]. Approximately 90 compact binary merger events have been observed thus far with the latest gravitational-wave transient catalog (GWTC-3) [2]. LIGO utilizes dual recycled, Fabry-Pérot-Michelson interferometers to measure gravitational-wave emissions from distant astrophysical sources [3]. Binary black hole mergers are characterized by two orbiting black holes that undergo distinct phases: an inspiral, merger, and ringdown phase that results in the formation of a single massive black hole [4]. Once the black holes form a binary system, through the emission of gravitational waves, the binary black holes lose orbital angular momentum and eccentricity which leads the black holes to inspiral in a quasi-circular orbit. As the orbiting black holes approach the merger, numerical relativity methods characterize this stage because the post-Newtonian expansion that describes the inspiral loses accuracy [5]. At the start of the merger, there is a plunge where the black hole horizons merge as their orbits become unstable. The resulting remnant black hole becomes stable in the ringdown stage and its gravitational-wave radiation is characterized by quasi-normal modes [6]. The gravitational-wave radiation provides the opportunity to test fundamental physics in the strong-field, highly dynamical regime of gravity which has been previously inaccessible in experimental tests of general relativity (GR) ([7].

LIGO's current population of binary merger events has been consistent with predictions of GR in the strong-field regime [8–10]. We can place constraints on alternative theories by inferring that GR is consistent with observations [11]. Einstein's theory of relativity has been tested extensively in the weak-field regime, yet theoretical expectations suggest that at high energies GR may break down [12]. This motivates testing theories around compact sources such as binary black hole mergers which involve stronger curvatures and shorter dynamical time scales [3, 12].

During the inspiral phase, gravitational-wave signals transition from the weak field to moderately strong field, and spacetime is violently curved when binaries merge [13]. The inspiral phase can be accurately

modeled with a post-Newtonian formalism [5]. The post-Newtonian formalism is a method for solving Einstein's field equations in the weak-field regime and it has been proven to be effective in describing energetic systems [14]. This method perturbatively expands the binary's evolution in powers of orbital frequency. Post-Newtonian phasing coefficients describe the physical effects in the relativistic dynamics of binaries, such as spin-spin interactions [15]. By focusing on the inspiral phase, we aim to look for deviations from GR by inferring the fractional deviations from the post-Newtonian phasing coefficients.

As LIGO becomes more sensitive, the number of binary mergers will grow which will allow for deviations to be more accurately constrained. By analyzing inspiral phase post-Newtonian coefficients for many gravitational-wave events, we are able to understand alternate theories whose coefficients vary in their post-Newtonian expression. The consistency of these coefficients with predictions of GR serve as a precise, independent test of the theory [10, 15].

Multi-parameter tests of GR consist of simultaneously inferring multiple post-Newtonian deviation parameters to search for deviations from GR. This general approach to jointly infer all parameters allows for us to constrain theories beyond GR, which can encompass deviations in more than one post-Newtonian phasing coefficient. To speed up this computationally intensive process, we apply a parameter estimation method, hybrid sampling, to jointly infer source and post-Newtonian deviation parameters. Hybrid sampling allows us to better understand the degeneracies in this high-dimensional parameter space. We apply a PCA which can be used to mitigate these degeneracies by transforming the deviation parameters into more informative parameters. However, these transformed parameters will not be used to constrain beyond GR theories in a hierarchical model due to individual gravitational-wave events needing a principal component basis across all observations.

In Section II, we describe applying the hybrid sampling method to astrophysical and deviation parameters in order to learn more about their correlations. After this, in Section III we explain our multi-parameter test including how injections were generated and a PCA application that allows us to learn more about where information is being carried in the parameter space. In Section IV, we apply hybrid sampling and a PCA to simulated gravitational-wave signals and demonstrate the presence of correlations between the deviation parameters. In Section V, the work completed over the summer is summarized and future directions are described.

II. Bayesian Inference

The objective in applying parameter estimation is to constrain the astrophysical parameters and the deviations from predictions of GR parameters in gravitational-wave sources. Bayesian inference allows us to recover the posterior probability distributions for the 15 parameters describing binary black hole mergers and the 10 deviation parameters describing their departure from GR. The posterior distributions of the source and deviation parameters are constructed using Bayes' theorem,

$$p(\theta|d,M) = \frac{\mathcal{L}(d|\theta,M)\pi(\theta|M)}{\mathcal{Z}(d|M)}\,, \tag{1}$$

where the 25 parameters θ are constrained given the observed strain data d and a model M [16]. The likelihood function, $\mathcal{L}(d|\theta,M)$, denotes the likelihood of observing the data given the parameter values and model. The prior distribution, $\pi(\theta|M)$, includes our assumptions about the parameters and is chosen to be uniform. The evidence, $\mathcal{Z}(d|M)$, is known as a normalization factor which entails the probability of observing the data given the model.

The likelihood describes the observations in different parameters, showing how well the model fits the data. It includes a noise model where the noise is assumed to be approximated by stationary Gaussian noise from LIGO's detectors [16]. The model M relates to a phenomenological model describing binary black hole merger waveforms that reflect our assumptions about the Universe, particularly about waveforms predicted by general relativity. Eq. 1 reflects the posterior distribution for the entire set of parameters. In obtaining the distribution on individual parameters, they must be marginalized over the other parameters. The resulting posterior distribution is high-dimensional and computationally expensive, therefore hybrid sampling is applied.

A. Hybrid Sampling

The first objective involves applying hybrid sampling via Bilby to jointly infer the 15 GR parameters of the binary black hole merger events in GWTC-3 and 10 post-Newtonian deviation parameters [17]. This method treats GR as the initial prediction in order to initialize the deviation parameter estimation. For each gravitational-wave signal, the data is sampled first using nested sampling via dynesty [18]. These nested samples initialize the walkers of a parallel-tempered Markov Chain Monte Carlo (MCMC) with the implementation of the package ptemcee in order to obtain generic, multi-dimensional samples [19, 20]. The hybrid sampling method is computationally efficient and has been empirically demonstrated to accurately recover posterior distributions [10]. By using nested sampling with only source parameters to seed a parallel-tempered ensemble MCMC with posterior estimates, hybrid sampling is able to efficiently explore the higher dimensional parameter space of an extended model that includes deviation parameters. This process is outlined in Fig. 1 below.

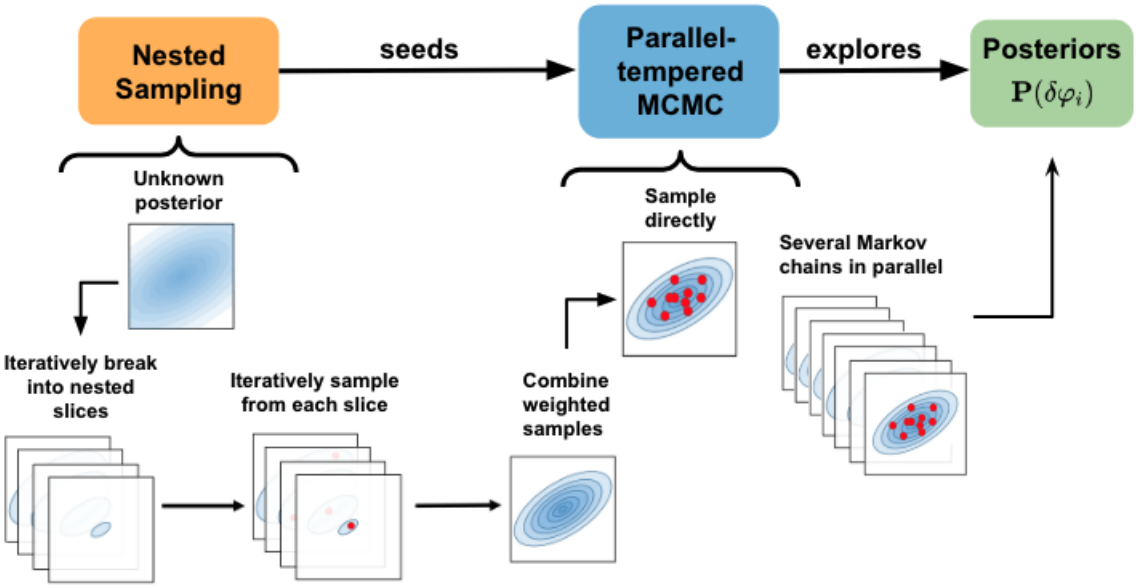

Figure 1: Schematic representation showing the steps involved in hybrid sampling to obtain posterior distributions. Nested sampling breaks the posterior into nested slices, samples from each slice, and recombines the samples to construct the original distribution with weights. Parallel-tempered MCMC directly samples from these nested samples and uses an ensemble of walkers, in parallel, to explore the posteriors at different temperatures.

1. Nested Sampling

The first step of hybrid sampling involves applying nested sampling to only the astrophysical parameters. Nested sampling approximates both the evidence and posterior distribution. Rather than directly sampling the posterior, nested sampling iteratively breaks up an unknown posterior into nested slices and samples from each slice. These samples are recombined to construct the original distribution with weights, resulting in combined weighted samples [18]. These samples from nested sampling are then used to seed the parallel-tempered MCMC.

More specifically, nested sampling takes random new points from the prior distribution. At each point, the lowest likelihood value is replaced from the set of random points with new samples drawn from the prior [16, 21]. This procedure continues until there is a random point that has a higher likelihood than the point that was replaced. For each removed point in a prior volume, the sum of likelihood with prior volume for each sample is calculated to estimate the evidence. Nested sampling is terminated when the replaced points at each iteration result in an integral encompassing the majority of the posterior [18].

2. Parallel-Tempered Monte Carlo Markov Chain

When incorporating a parallel-tempered MCMC, both the astrophysical and deviation parameters are being sampled. Several parallel Markov chains directly sample from the resulting combined nested samples described in Sec. II A 1. These walkers, in parallel, explore the posteriors at different temperatures, denoted by $\beta_T = \frac{1}{T}$. The posterior distributions at various temperatures from this ensemble MCMC method is

$$p_{\beta_T}(\theta|d) = \frac{\mathcal{L}^{\beta_T}(d|\theta)\pi(\theta)}{\mathcal{Z}^{\beta_T}(d)}, \tag{2}$$

where $\mathcal{L}^{\beta_T}$ is the tempered likelihood surface [10]. When the temperature approaches infinity, the tempered posterior reaches the prior. Higher temperatures result in the posterior distribution being easier to sample with MCMC, due to the peaks in the likelihood distribution becoming broader [20]. The ensemble of walkers can easily explore the prior volume and convergence time is reduced by allowing walkers to jump between different temperatures [10]. This method efficiently allows for the ensemble of walkers to accurately estimate the posterior distribution in less iterations and at any step, the ensemble is representative of the posterior [10]. By applying hybrid sampling, degenerate parameter spaces can be explored.

B. Hierarchical Inference

After generating posterior distributions for all the astrophysical and deviation parameters, we plan on applying a hierarchical approach to test specific theories using all the possible deviations from GR for each gravitational-wave event. This hierarchical procedure involves combining multiple gravitational wave events and marginalizing over individual event parameters [9]. In combining events hierarchically and sampling the hyperposterior, we are able to learn more about the underlying population parameters. These population parameters can describe the coupling coefficients of specific theories beyond GR. The hierarchical inference method further entails using a Gaussian Mixture Model (GMM), which is a computationally inexpensive density estimation procedure [22]. The GMM estimates the posterior probability densities of each individual event. This allows for the likelihood functions for each event to be efficiently evaluated [9].

III. Modeling Tests of GR Deviations

Parameterized tests of GR involve searching for deviations in the post-Newtonian phasing coefficients in the phase evolution of signals. The deviations from GR are modeled by

$$\varphi_i \to \varphi_i^{GR}(1 + \delta\varphi_i), \tag{3}$$

where $\varphi_i^{GR} = \{\varphi_{-2}, \varphi_0, \varphi_1, \varphi_2, \varphi_3, \varphi_4, \varphi_{5L}, \varphi_6, \varphi_{6L}, \varphi_7\}$ and $\delta\varphi_i$ denotes the dimensionless fractional deviation parameters [15]. When $\delta\varphi_i$ are zero, it corresponds to there being no deviation from GR.

For our source model, the post-Newtonian parameterization of the phase evolution during the inspiral phase of the general relativistic waveform in the frequency domain is

$$\Phi(f) = 2\pi f t_c - \phi_c - \frac{\pi}{4} + \frac{3}{128} \times \sum_{k=0}^{7} \frac{1}{\eta^{k/5}} \Big(\varphi_k + \varphi_{k,l} \ln \tilde{f}\Big) \tilde{f}^{(k-5)/3}, \tag{4}$$

where t_c is the time and ϕ_c is the phase when the binary black holes coalesce, $\eta = m_1 m_2/M^2$ is the symmetric mass ratio of the system, f is the frequency, and $\tilde{f}$ is the frequency scaled by $\pi G\mathcal{M}(1+z)f/c^3$[23].

Previous analyses have modified a single deviation parameter at a time which has proven to be effective in finding deviations that involve multiple phasing coefficients, however the effectiveness of multi-parameter tests can be improved [10, 11]. A multi-parameter test of GR is conducted to obtain generic deviation parameters in order to map them to specific theories and constrain their coupling coefficients.

A. Injection Generation

Waveforms were generated using a phenomenological waveform model, IMRPhenomPv2, to conduct the parameter estimation mentioned in Sec. II. The priors for the deviation parameters are shown in Table 1. For this analysis, we vary $\delta\varphi_2$ as a test when injecting beyond GR signals into simulated noise from LIGO's Hanford detector.

Parameter	Prior
$\delta\varphi_0$	$\mathcal{U}$(-2, 2)
$\delta\varphi_1$	$\mathcal{U}$(-4, 4)
$\delta\varphi_2$, $\delta\varphi_3$, $\delta\varphi_4$, $\delta\varphi_{5L}$	$\mathcal{U}$(-8, 8)
$\delta\varphi_6$	$\mathcal{U}$(-10, 10)
$\delta\varphi_{6L}$, $\delta\varphi_7$	$\mathcal{U}$(-40, 40)

Table 1: Prior distributions for the deviation parameters which are uniform distributions $\mathcal{U}(x, y)$, where x is the lower limit and y is the upper limit of the distribution.

Signal-to-noise ratio (SNR) and overlap cuts were applied to produce 10 injection parameters that more closely align with real gravitational wave signals and do not significantly deviate from GR. The SNR cut involved using the optimal SNR from the Hanford interferometer at a sampling frequency of 1024 Hz, reference frequency set to 20 Hz, and for a duration of 8 seconds. Injections were randomly sampled until the optimal SNR > 20, to ensure the gravitational wave signals were not buried by the detector's noise. The cut was made on the inspiral SNR, computed from a frequency range of 20 Hz to the frequency of the innermost stable circular orbit,

$$f_{ISCO} = \frac{c^3}{6\sqrt{6}G(m_1 + m_2)} \tag{5}$$

where m_1 and m_2 are the component masses. In this context, the innermost stable circular orbit is right before the binary black holes plunge and this cut allows us to capture the inspiral phase.

We apply an overlap cut between beyond GR signals and their associated GR signal to constrain the signals to be similar. The overlap $O > 0.9$,

$$O = \Big| \frac{\langle \tilde{h}_{GR}, \tilde{h}_{BGR} \rangle}{\sqrt{\langle \tilde{h}_{GR}, \tilde{h}_{GR} \rangle \langle \tilde{h}_{BGR}, \tilde{h}_{BGR} \rangle}} \Big| \tag{6}$$

was derived where $\tilde{h}_{GR}$ is the +-polarization of the GR waveform in the frequency domain and $\tilde{h}_{BGR}$ is the +-polarization of the beyond GR waveform [10]. The inner products between the waveforms are weighted with the power spectral density from the Hanford detector. The same source parameters were used in $\tilde{h}_{GR}$ and $\tilde{h}_{BGR}$. As seen in Fig. 2, the waveforms in the time domain with these cuts appear to resemble real gravitational wave signals. In this example, the beyond GR waveform had a deviation in $\delta\varphi_2$.

B. Principal Component Analysis

To further understand the underlying correlations between the deviation parameters, a Principal Component Analysis (PCA) decomposition is applied to create new deviation parameters. The resulting posterior distributions from jointly inferring all the deviation parameters, is used to compute a covariance matrix consisting of the covariance between pairs of deviation parameters [15]. A linear transformation is applied to create the PCA parameters,

$$\delta\varphi^{(i)}_{PCA} = \sum_k \alpha^{ik} \delta\varphi_k, \tag{7}$$

which results in linear combinations of the original deviation parameters with the components of the transformation matrix. The coefficients α^{ik} are the eigenvectors of the transformation matrix where i is the number corresponding to the PCA parameters. The coefficients and deviation parameters are summed over k, the number of deviation parameters. The leading PCA parameters are expected to carry the most information.

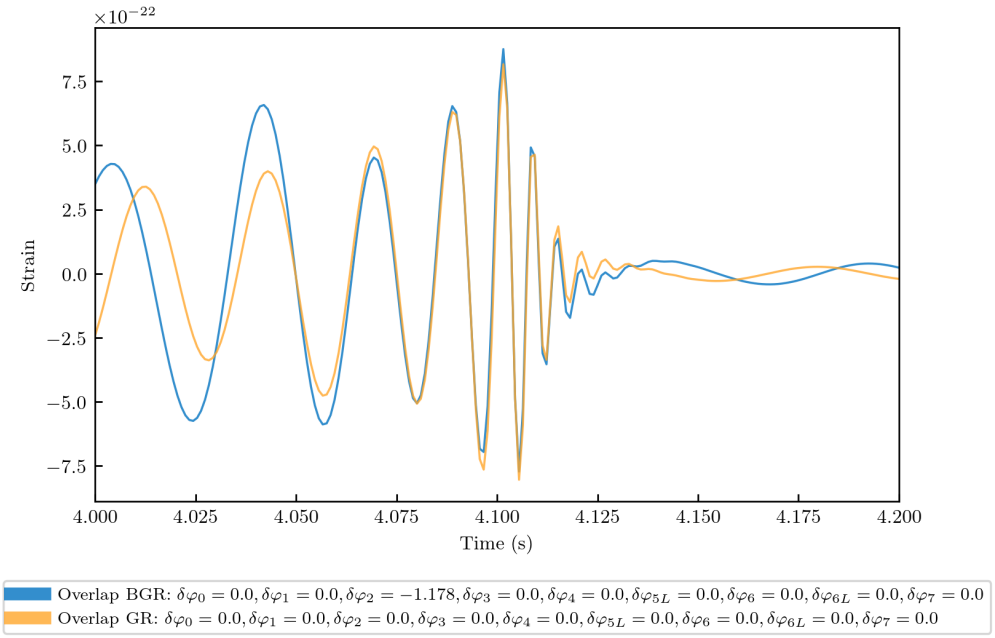

Figure 2: Beyond GR strain in the time domain for an injection that includes the SNR and overlap cuts and its associated GR waveform. There is a deviation in $\delta\varphi_2$ for the beyond GR waveform.

In addition, the PCA parameters are not used for hierarchical applications because a common eigenbasis is needed for all events, resulting in difficulty mapping to specific theories beyond GR.

IV. Results

A. Parameter Estimation

A parameter estimation run was made with the SNR and overlap cuts, as described in Sec. III A, and adjusted parallel-tempered MCMC parameters. The number of steps used by ptemcee increased to 200 and the unburnt chains were stored in the result. Figure 3 shows the improved marginal and joint distributions for an arbitrary example of injection parameters. The expected correlation between $\mathcal{M}$ and q is seen. The marginal distributions for each of the displayed parameters have converged towards their true parameters. A roughly positive correlation is also seen between $\delta\varphi_2$ and $\delta\varphi_3$, which describe the early inspiral regime.

Normalized likelihoods were evaluated to try to understand the posterior distribution of $\delta\varphi_4$. These likelihood values were calculated given the source parameters that correspond to a particular likelihood value, such as the maximum likelihood value, along the $\delta\varphi_4$ prior range. In Fig. 4 the parameters from the maximum, minimum, and two randomly sampled likelihood values were calculated to illustrate the likelihood surface. The likelihood value is plotted on the y-axis and a range of $\delta\varphi_4$ values, spanning the prior range, is on the x-axis. The dotted black line indicates the true value of $\delta\varphi_4$. The curves show the maximum, minimum, and two random likelihoods with their proportional likelihood distribution. There is a cut off at the prior bounds for $\delta\varphi_4$. The resulting likelihood distributions appear Gaussian which indicates that there are potentially underlying correlations in the marginal posterior distributions that are not being seen in our corner plot.

B. PCA Decomposition

By applying a PCA decomposition to the 10 deviation parameters from the hybrid sampling run described in the previous Sec. IV A, we learned where most of the information in our posteriors is coming from. As expected, the first two parameters $\delta\varphi^0_{PCA}$ and $\delta\varphi^1_{PCA}$ are the most informative. As seen in Fig. 5,

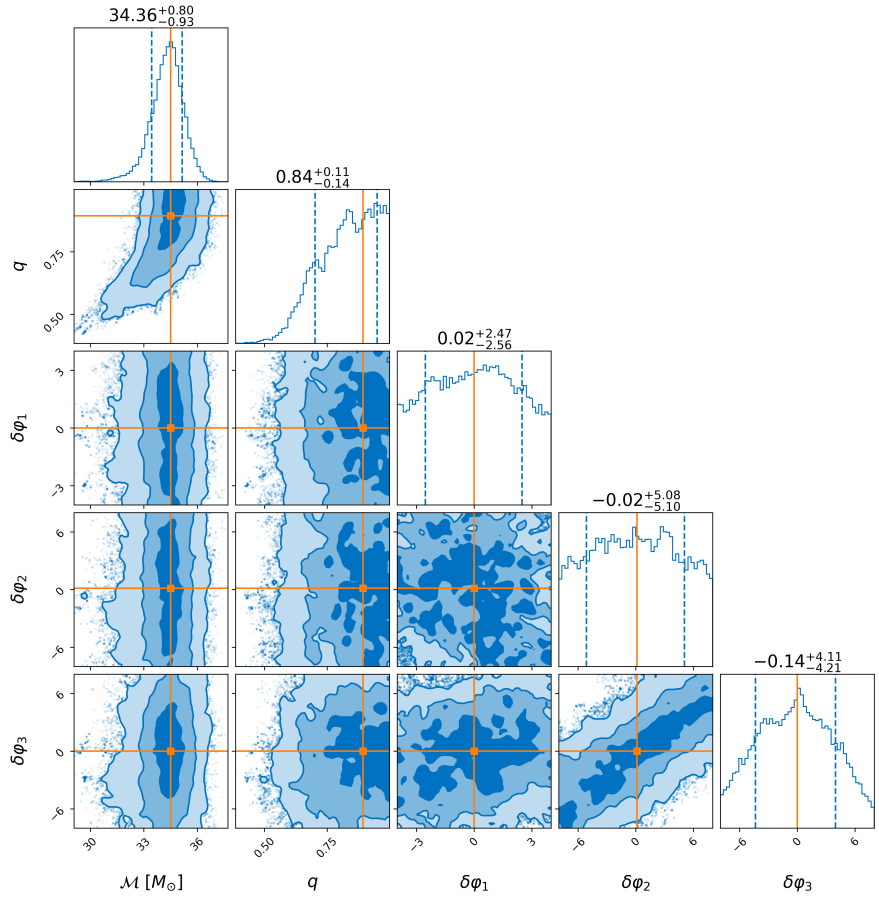

Figure 3: Marginal and joint posterior distributions of the $\mathcal{M}$, q, and deviation parameters resulting from the SNR and overlap cuts as well as improved ptemcee parameters. The contours denote the 1, 2, and 3σ confidence intervals. The orange line indicates the true value for each parameter.

the marginal distributions are wider the farther in the corner plot that they are from the two leading PCA parameters because these leading parameters already contain the most of the information. The marginal distributions of each PCA parameter consistently converge at zero, except $\delta\varphi^0_{PCA}$ because $\delta\varphi_2$ is dominating the eigenspace. The correlations are generally removed, as expected, in order to understand more about where the information is being carried in the parameter space.

V. Conclusions

In working towards constraining specific theories beyond GR, we applied hybrid sampling to the deviation parameters associated with the inspiral of binary black hole mergers at the same time. This resulted in obtaining posterior distributions for the 25 parameters describing the source and deviations, and allowed us to learn more about the correlations amongst the source and deviation parameters. To better understand these correlations and create a more effective multi-parameter test, we then applied PCA to the marginal posterior distributions of the deviation parameters which recast these correlations. This showed that most of the information from the data is coming from the two leading PCA parameters.

This result motivates our next step to apply both hybrid sampling and a PCA to real gravitational-wave signals. Then, the hybrid sampling results from individual events and a hierarchical model consisting of theories of gravity can be applied. In the future, this will allow us to try to constrain the bounds on coupling coefficients characterizing these beyond GR theories which are mapped out via a parameterized

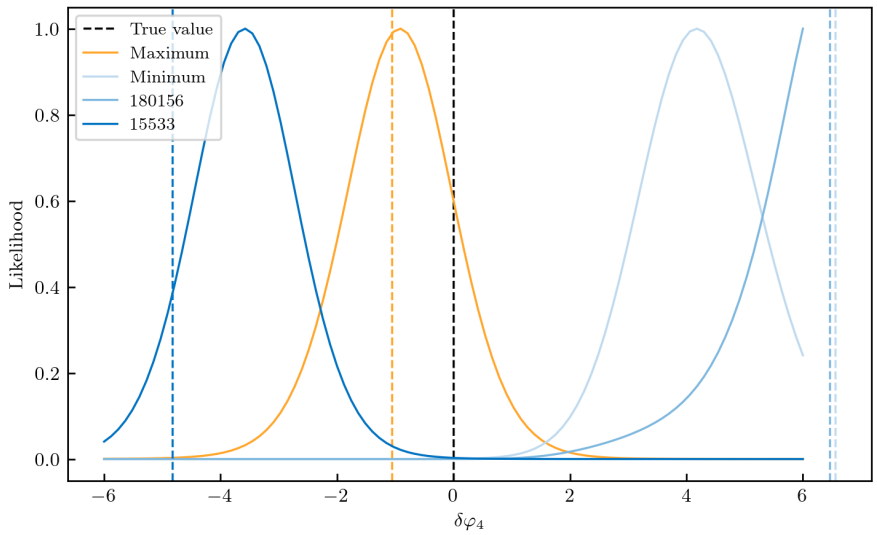

Figure 4: Normalized likelihoods of $\delta\varphi_4$ over the prior range. The normalized likelihood is plotted on the y-axis and a range of $\delta\varphi_4$ values, spanning the prior range, is on the x-axis. The dotted black line indicates the true value of 0. The curves show the maximum, minimum, and two random likelihood values with their proportional likelihood distribution.

post-Einsteinian framework [24].

Acknowledgements

I am very grateful towards my mentor, Ethan Payne, for his guidance and support this summer. I would like to thank Alan Weinstein for organizing the LIGO SURF program. This work was supported by the National Science Foundation Research Experience for Undergraduates (NSF REU) program, the LIGO Laboratory Summer Undergraduate Research Fellowship program (NSF LIGO), the Victor M. Blanco Fellowship, and the California Institute of Technology Student-Faculty Programs.

References

[1] B. P. Abbott et al. LIGO: The Laser interferometer gravitational-wave observatory. *Rept. Prog. Phys.*, 72:076901, 2009.

[2] R. Abbott et al. GWTC-3: Compact Binary Coalescences Observed by LIGO and Virgo During the Second Part of the Third Observing Run. 11 2021.

[3] B. P. Abbott et al. Tests of general relativity with GW150914. *Phys. Rev. Lett.*, 116(22):221101, 2016. [Erratum: Phys.Rev.Lett. 121, 129902 (2018)].

[4] J. Meidam et al. Parametrized tests of the strong-field dynamics of general relativity using gravitational wave signals from coalescing binary black holes: Fast likelihood calculations and sensitivity of the method. *Phys. Rev. D*, 97(4):044033, 2018.

[5] L. Blanchet. Gravitational Radiation from Post-Newtonian Sources and Inspiralling Compact Binaries. *Living Reviews in Relativity*, 17(1):2, December 2014.

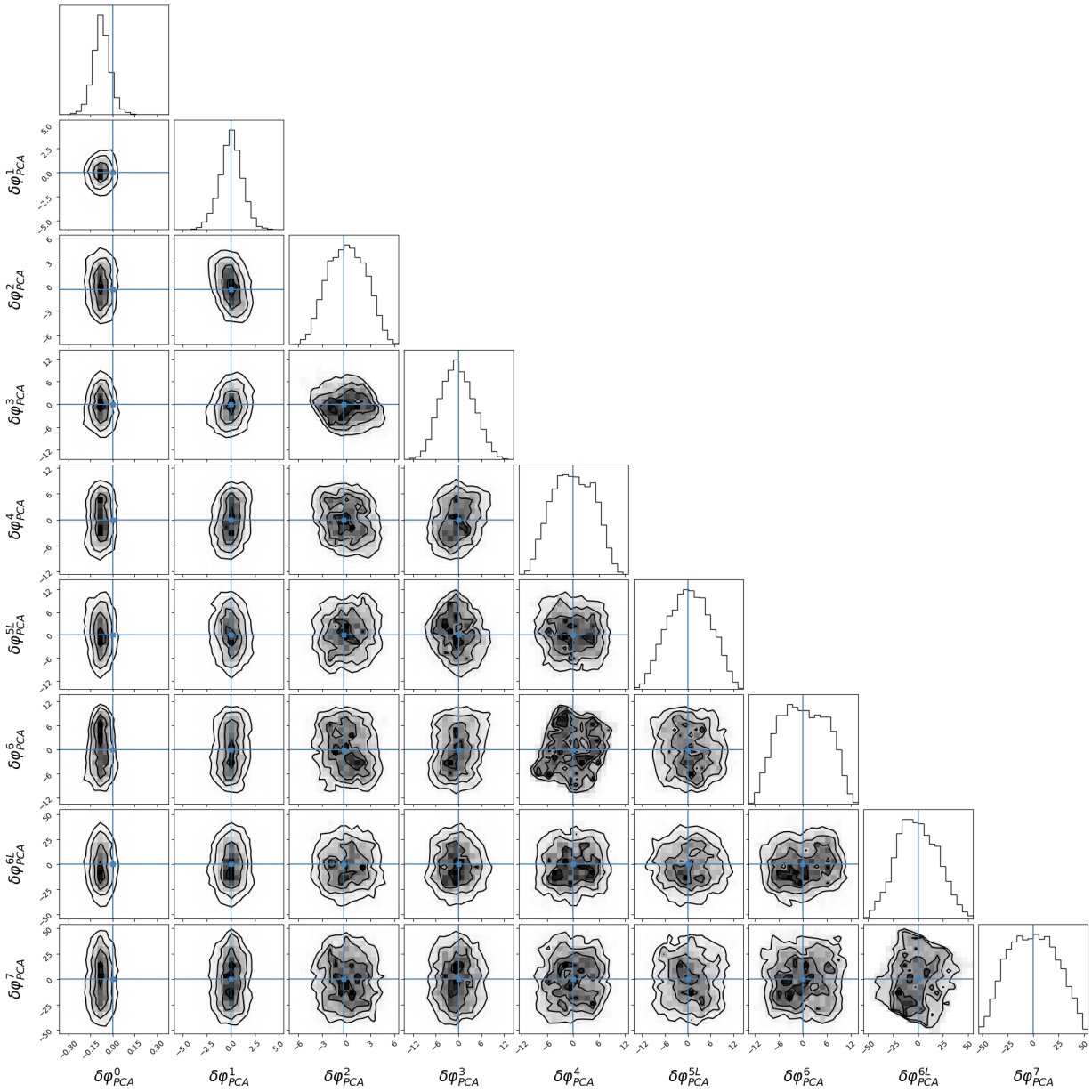

Figure 5: Marginal and joint distributions of the 10 deviation parameters generated from applying PCA. The contours denote the 1, 2, and 3σ confidence intervals. The blue line indicates the true value for each parameter.

[6] R. Abbott et al. Tests of general relativity with binary black holes from the second LIGO-Virgo gravitational-wave transient catalog. *Phys. Rev. D*, 103(12):122002, 2021.

[7] H. Narola, S. Roy, and A. S. Sengupta. Beyond general relativity: Designing a template-based search for exotic gravitational wave signals. *PhRvD*, 107(2):024017, January 2023.

[8] B. P. Abbott et al. Tests of General Relativity with the Binary Black Hole Signals from the LIGO-Virgo Catalog GWTC-1. *Phys. Rev. D*, 100(10):104036, 2019.

[9] J. Golomb and C. Talbot. Hierarchical Inference of Binary Neutron Star Mass Distribution and Equation of State with Gravitational Waves. *ApJ*, 926(1):79, February 2022.

[10] N. E. Wolfe, C. Talbot, and J. Golomb. Accelerating tests of general relativity with gravitational-wave signals using hybrid sampling. *Phys. Rev. D*, 107(10):104056, 2023.

[11] R. Abbott et al. Tests of General Relativity with GWTC-3. 12 2021.

[12] E. Berti et al. Testing General Relativity with Present and Future Astrophysical Observations. *Class. Quant. Grav.*, 32:243001, 2015.

[13] K. Yagi, L. C. Stein, N. Yunes, and T. Tanaka. Erratum: Post-Newtonian, quasicircular binary inspirals in quadratic modified gravity [Phys. Rev. D 85, 064022 (2012)]. *PhRvD*, 93(2):029902, January 2016.

[14] C. M. Will. Inaugural Article: On the unreasonable effectiveness of the post-Newtonian approximation in gravitational physics. *Proceedings of the National Academy of Science*, 108(15):5938–5945, April 2011.

[15] M. Saleem, S. Datta, K. G. Arun, and B. S. Sathyaprakash. Parametrized tests of post-Newtonian theory using principal component analysis. *PhRvD*, 105(8):084062, April 2022.

[16] E. Thrane and C. Talbot. An introduction to bayesian inference in gravitational-wave astronomy: Parameter estimation, model selection, and hierarchical models. *Publications of the Astronomical Society of Australia*, 36, 2019.

[17] G. Ashton et al. BILBY: A user-friendly Bayesian inference library for gravitational-wave astronomy. *Astrophys. J. Suppl.*, 241(2):27, 2019.

[18] J. S. Speagle. DYNESTY: a dynamic nested sampling package for estimating Bayesian posteriors and evidences. *MNRAS*, 493(3):3132–3158, April 2020.

[19] D. Foreman-Mackey, D. W. Hogg, D. Lang, and J. Goodman. emcee: The MCMC Hammer. *PASP*, 125(925):306, March 2013.

[20] W. D. Vousden, W. M. Farr, and I. Mandel. Dynamic temperature selection for parallel tempering in Markov chain Monte Carlo simulations. *MNRAS*, 455(2):1919–1937, January 2016.

[21] J. Skilling. Nested sampling for general bayesian computation. *Bayesian Analysis*, 1:833–859, 2006.

[22] C. Talbot and E. Thrane. Flexible and Accurate Evaluation of Gravitational-wave Malmquist Bias with Machine Learning. *ApJ*, 927(1):76, March 2022.

[23] D. Psaltis, C. Talbot, E. Payne, and I. Mandel. Probing the black hole metric: Black hole shadows and binary black-hole inspirals. *PhRvD*, 103(10):104036, May 2021.

[24] S. Tahura and K. Yagi. Parametrized post-einsteinian gravitational waveforms in various modified theories of gravity. *Physical Review D*, 98(8), October 2018.